International Journal of Microwave and Wireless Technologies

cambridge.org/mrf

From bulk toward micro-structured TiO_2 ceramics for all-dielectric metamaterials at terahertz frequencies: what process?

Djihad Amina Djemmah[1], Delphine Gourdonnaud[2], Feriel Laourine[1], David Bouville[1], Fayçal Bouamrane[3], Jean-François Roux[4], Pierre-Marie Geffroy[2] and Eric Akmansoy[1]

[1]Centre de Nanosciences et de Nanotechnologies, university. Paris-Saclay, UMR 9001, CNRS, 10 bd T. Gobert, Palaiseau, France; [2]IRCER, university. de Limoges, CNRS, UMR 7315, 12 rue Atlantis, Limoges, France; [3]Laboratoire Albert Fert, CNRS/THALES, UMR 137, 1st Avenue Augustin Fresnel, Palaiseau, France and [4]CROMA, university. Grenoble Alpes, university. Savoie Mont-Blanc CNRS, UMR 5130, Grenoble, France

Research Paper

Cite this article: Djemmah DA, Gourdonnaud D, Laourine F, Bouville D, Bouamrane F, Roux J-F, Geffroy P-M, Akmansoy E (2025) From bulk toward micro-structured TiO_2 ceramics for all-dielectric metamaterials at terahertz frequencies: what process? *International Journal of Microwave and Wireless Technologies* **17**(5), 881–891. https://doi.org/10.1017/S1759078725101931

Received: 18 December 2024
Revised: 11 July 2025
Accepted: 20 July 2025

Keywords:
Ceramics; Dielectrics; Metamaterials; Negative refractive index; Processes; Terahertz

Corresponding author: Eric Akmansoy; Email: eric.akmansoy@universite-paris-saclay.fr

Abstract

In this study, we aimed to develop high permittivity TiO_2 ceramics ideal for the fabrication of all-dielectric metamaterials (ADM) operational in the terahertz frequency. TiO_2 ceramic pellets have been fabricated from a commercial powder. A comparative analysis was conducted between spark plasma sintering (SPS) and conventional sintering process. Characterizations were then carried out in the range of 0.2–1.4 THz using THz time-domain spectroscopy. We observed that the samples fabricated by the SPS and post-annealing treatment exhibit a high permittivity associated with minimal loss ($\varepsilon' \simeq 100$ and $\tan\delta < 0.015$). These characteristics make these samples optimal candidates for achieving a negative or near-zero effective index in all-dielectric metamaterials. In addition, four micro-structuring processes were investigated to produce ADM operating in the terahertz range from the ceramics:

(i) micro-molding,
(ii) direct TiO_2 etching by inductively coupled plasma,
(iii) saw cutting and
(iv) femtosecond laser etching.

Introduction

Metamaterials (MM) display unique phenomena, such as negative index, because of their engineered sub-wavelength structure. Our aim is to realize an all-dielectric metamaterial (ADM) operating in the terahertz (THz) range [1]. Indeed, conventional MMs are built around a metallic unit cell, having a complex geometry, and they consequently suffer from ohmic losses that increase with frequency [2]. Differently, the unit cell of ADMs consists of two high permittivity resonators with simple geometry. The incident electromagnetic (EM) field excites the first two Mie resonances, which results in resonant effective permeability and permittivity, respectively. The superposition of the latter may lead to a negative or near-zero effective index n_{eff}. Ceramics, particularly those with high permittivity and low loss [3], are suitable for ADMs. In the terahertz range, the bulk ceramics has to be structured to the tens micrometers scale, with a precision of the micron, so as to sustain the resonances. Besides, THz radiation, defined between 0.1 and 10 THz, has various applications including imaging and sensing, as it provides unique physical phenomena. The targeted frequencies are 0.3 and 0.6 THz, because they correspond to windows of atmospheric transmission. We produced samples using TiO_2 ceramic, chosen for its high permittivity and low loss. The bulk TiO_2 samples were fabricated from commercial powders and sintered using two different processes: conventional and spark plasma sintering (SPS). These samples were then characterized in the 0.2–1.4 THz range using THz time-domain spectroscopy (THz-TDS). We further looked for the best way to structure the bulk TiO_2 ceramics at the micron scale, to realize an ADM operating at THz, and then considered four different micro-structuring processes:

(i) micro-molding,
(ii) direct TiO_2 etching by inductively coupled plasma (ICP),
(iii) saw cutting and
(iv) femtosecond laser etching.

© The Author(s), 2025. Published by Cambridge University Press in association with The European Microwave Association.

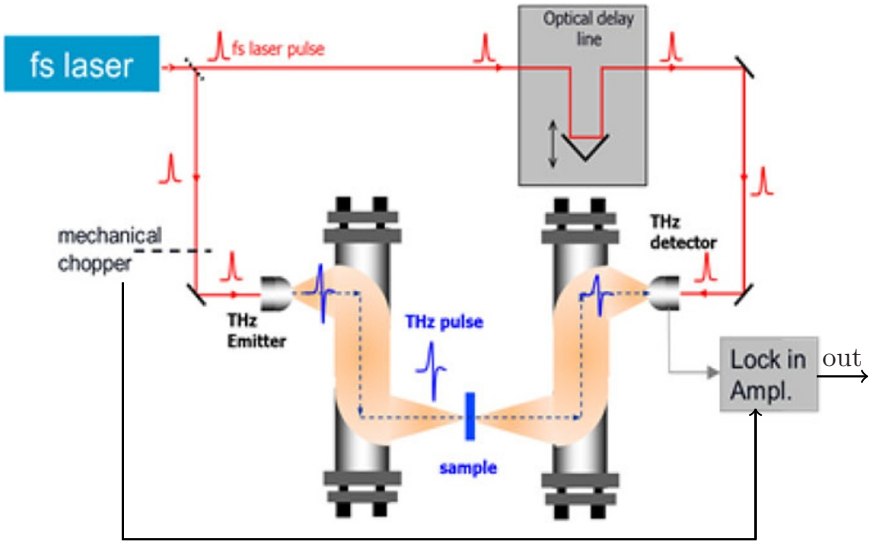


Figure 1. Schematic diagram of the experimental THz time-domain spectroscopy (THz-TDS) setup.

Specifically, we employed micro-machining for the devices aimed at 0.3 THz, whereas ICP etching was adopted for that targeting 0.6 THz. This manuscript reports on an exploratory work to find out a process to shape the bulk TiO_2 material at the tens of micrometers with a one micrometer resolution. Currently, TiO_2 is shaped at the nanoscale or when it is in the form of a film a few hundred nanometers thick [4–6]. An earlier version of this paper was presented at the 18th Conference of Antennas and Propagation (EuCAP 2024) and was published in its Proceedings [7].

Experimental methods

Fabrication processes of the bulk material

The bulk TiO_2 ceramic was obtained through two distinct sintering process: conventional sintering and SPS. In the conventional sintering process, TiO_2 powder is compacted using a die of 10 mm diameter under a compressive pressure of 50 MPa to form green compacts. These compacts are then sintered at 1550°C during 30 min to produce a dense material.

Differently, during the SPS process, the TiO_2 powder is placed in an 8 mm diameter graphite die. The material is then sintered using a high-intensity pulsed current at a temperature of 1150°C and under a pressure of 10 MPa for a period of 5 minutes. Following the sintering processes, half of the samples were annealed in an ambient atmosphere, at temperatures set between 950° and 1100°C during 60 hours. Lastly, the TiO_2 ceramic pellets were precisely polished to achieve a thickness ranging from 300 to 500 μm.

THz characterization

For the characterization of the polished ceramic pellets, we used a commercial *Terapulse Lx* spectrometer from TeraView™ [8]. This system is based on a femtosecond fiber laser operating at a repetition rate of 80 MHz. Its optical pulses are split into two paths by a beam splitter. One of these paths directs the pulses to the THz emitter (a photoconductive antenna), while the other leads to the THz detector. During measurement, the THz beam from the emitter passes through the sample located in a dry air chamber, in which the relative humidity is maintained below 10%. This beam is guided

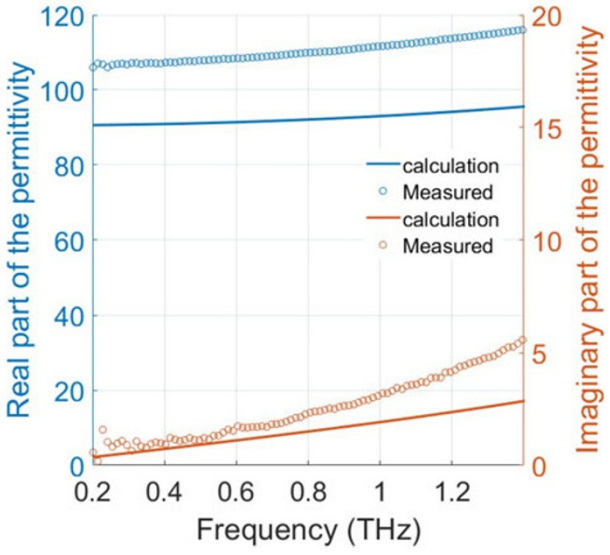


Figure 2. Comparison of the THz-TDS experimental data (circles) with those of the FPSQ model (solid line): real and imaginary parts of the dielectric function ε^*.

by four parabolic mirrors and its interaction with the sample is sampled using an optical delay line. The THz detector records the electric field as a function of time. This temporal signal then undergoes a Fast Fourier Transform to obtain the optical spectra. By comparing this transmitted signal with a reference signal, obtained without the sample, the spectra of the two signals can be calculated. From this data, we extract the complex refractive index $n+i\kappa$ of the sample. Eventually, these values are used to determine the complex permittivity $\varepsilon^* = \varepsilon' + i\varepsilon''$ [9, 10]. Before the characterization of the samples, the setup has been calibrated by the means of a BK7 glass plate. The schematic of this experimental setup is shown in Fig. 1 (A top view is shown in fig. 1 in the supplementary material file).

The experimental results, reported in Fig. 2, are in good agreement with those of [3, 11]; they are also in good agreements with the Four Parameters Semi-Quantum (FPSQ) model, which has been calculated using the permittivity ϵ' of rutile (001) single crystal, which is isotropic. [12, 13] In the concerned frequency range,

https://doi.org/10.1017/S1759078725101931 Published online by Cambridge University Press

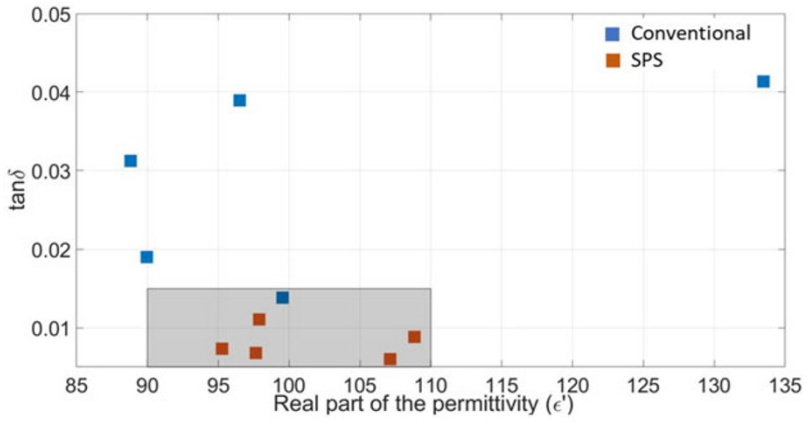


Figure 3. Loss $\tan\delta$ as a function of the real part ε' of the permittivity at 0.3 THz for all the TiO_2 samples. Conventional sintering is indicated in blue, whereas SPS is in red. The shaded area highlights the samples whose the loss tangent is $\tan\delta \leq 0.015$ and the real permittivity is between 90 and 110. $\tan\delta \leq 0.015$ is easily achieved by SPS.

the real part ε' of the permittivity linearly increases with the frequency, and the imaginary part ε'' almost linearly increases with the frequency, but it is higher than that of the FPSQ model. We assume that this is due to the concentration of oxygen vacancies V_O and Ti_3^+ ions [14]. Moreover, the fabricated TiO_2 pellets are made from powder are polycrystalline, which means they are composed of numerous crystalline grains with random orientations. The interfaces between them, as well as possible impurities and defects in the material, may induce additional dielectric behaviors not accounted for in an idealized semi-quantum model (see also [13]).

Results and discussion

Influence of the type of sintering on the dielectric properties

For the successful realization of an ADM, we thus seek the most suitable process for manufacturing TiO_2 pellets with a high permittivity ($\varepsilon' \simeq 100$) and a minimal loss factor ($\tan\delta \lesssim 0.02$)) from commercial powders [13]. We explored both conventional sintering and SPS.

A total of ten samples were synthesized – one half using conventional sintering and the other half using SPS. The characterization by Time Domain THz Spectroscopy (TDS-THz), as reported in Fig. 3, shows that the samples produced by SPS (indicated in red) exhibit improved properties compared with those produced by conventional sintering (indicated in blue). XRD characterizations were carried out on some of the samples, showing that the synthesized TiO_2 ceramic is of the rutile type.

Influence of annealing treatment on the dielectric loss

As the loss is an essential parameter to obtain the Mie resonances, we investigated the effect of annealing on this parameter. Twelve samples of two types were manufactured by pair under the same conditions (indicated by the same color), half annealed (indicated by square), half not (indicated by triangles) (see Fig. 4). The plot clearly shows that the annealed samples exhibit significantly lower dielectric losses ($\tan\delta \leq 0.015$) and a real part of permittivity between 90 and 110 at 0.3 THz. This result highlights the importance of this post-process, because during the SPS process, the material is subjected to high temperatures and pressure, which can result in the formation of defects. The latter can significantly affect the dielectric properties of the material. Annealing allows for

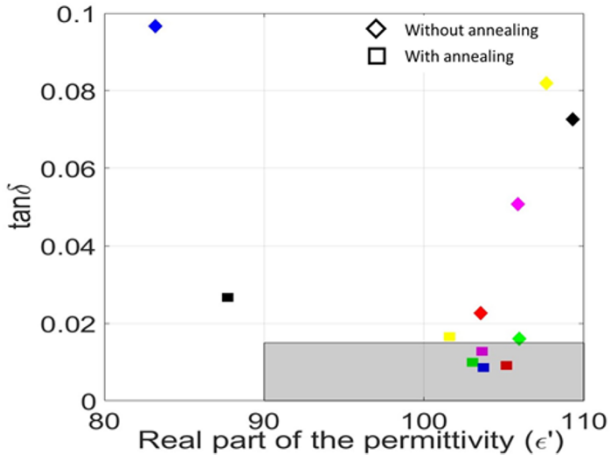


Figure 4. The loss ($\tan\delta$) as a function of real part (ε') of the permittivity at 0.3 THz of TiO_2 samples elaborated by SPS with annealing (squares) and without annealing (triangles). The shaded area highlights the loss range corresponding to $\tan\delta < 0.015$ as well as the real permittivity value range of ε' between 90 and 110, necessary to excite the Mie resonances.

reducing the concentration of defects in the material, particularly in terms of Ti_3^+ anomalies and oxygen vacancies.

Numerical simulation of the all-dielectric metamaterials

Based on these experimental results, we designed and simulated ADMs operating at THz frequencies. Their EM properties have been numerically simulated by the means of the Lumerical™ software, that involves the finite-difference time domain (FDTD) method; it yields the *S*-parameters from which the EM effective parameters (permeability, permittivity and index) are extracted. The simulations were specifically based on the measured characteristics of a TiO_2 sample whose loss is $\tan\delta = 0.015$ at 0.3 THz, and its permittivity $\varepsilon_r = 102$. The elementary cell of the ADM comprises two 2D cylinders of TiO_2, one having a rectangular cross-section (58 μm × 110 μm) and the other having a square cross-section (110 μm × 110 μm). The cylinders are arranged in a periodic pattern with a period of 200 μm. The incident field is Transverse Electric (mode TE), the electric field being perpendicular to the axis of the cylinders. A schematic of the ADM is shown in Fig. 5.

https://doi.org/10.1017/S1759078725101931 Published online by Cambridge University Press

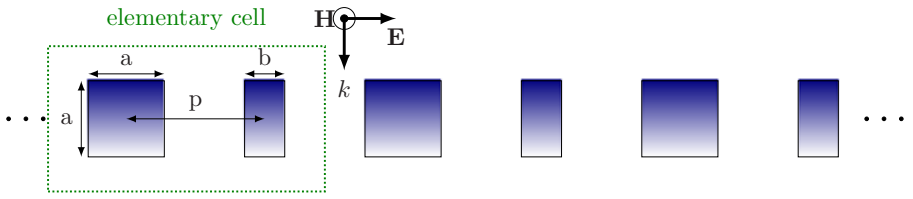


Figure 5. Schematic of the 2D all-dielectric metamaterial. It is a periodic device, whose elementary cell consists of two height permittivity resonators, one having a rectangular cross-section ($a \times b$) and the other having a square cross-section ($a \times a$). The cylinders are arranged with a period p. The incident EM field is transverse electric.

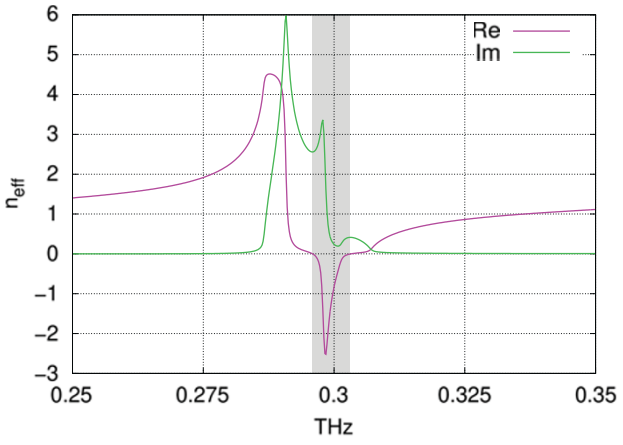


Figure 6. Numerical simulation of the effective index of an all-dielectric metamaterial. The dielectric properties used for the computation are derived from one of the characterized TiO_2 samples: permittivity $\varepsilon' \simeq 102$ and losses $\tan\delta \simeq 0.015$ at 0.3 THz. The shaded region highlights the frequency range where the effective index is negative; its minimum is $n_{eff_{min}} = -2.52$ at 0.298 THz and its bandwidth is 7.1 GHz.

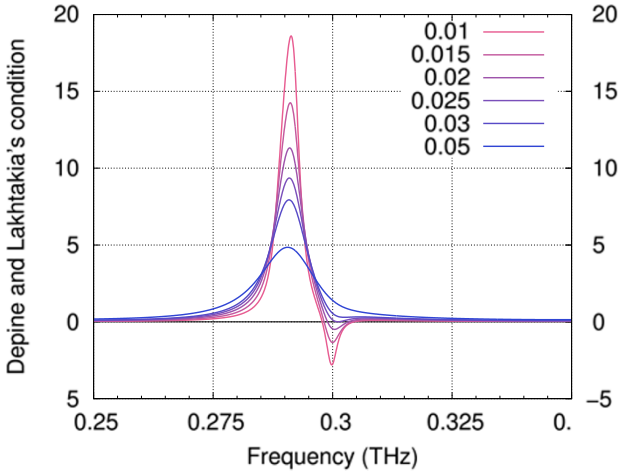


Figure 7. Depine and Lakhtakia's condition as the loss is varied from $\tan\delta = 0.01$ to 0.05. Effective negative index is only achieved as $\tan\delta \leq 0.02$.

The dimensions of these 2D resonators have been deduced from the Cohn's model, which gives the frequency of the modes by the relation [15]:

$$f_{mn} = \frac{c}{2\sqrt{\varepsilon_r}}\sqrt{\left(\frac{m}{a}\right)^2 + \left(\frac{n}{b}\right)^2}, \qquad (1)$$

where m and n are integers, and a and b are the dimensions of the sides of the 2D resonators. As we consider the first two modes of

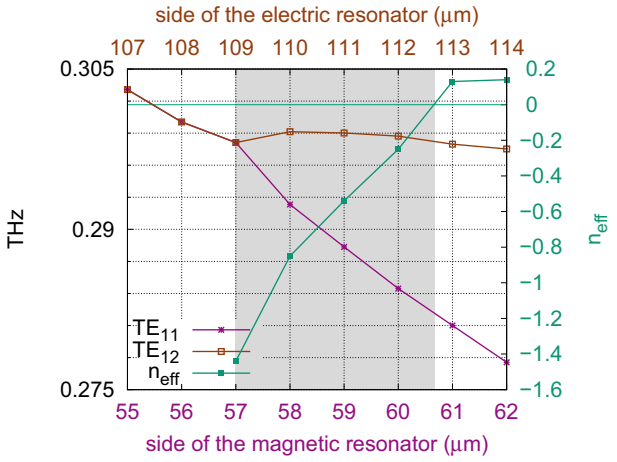


Figure 8. Frequency of the minima of the S_{21}-parameter of the first two modes TE_{11} and TE_{12} in function of the side of the resonators. The frequencies of the two modes come closer as the same side of the resonators diminishes until they become equal; the two modes are then degenerated. Simultaneously, the effective index decreases, going from near zero values to negative ones (green curve). When the modes are degenerated, it is no longer defined.

Mie resonances, $m = n = 1$ and $m = 1, n = 2$ in the elementary cell, the first mode (denoted TE_{11}) being the magnetic one and the second (denoted TE_{12}), the electric one. Their respective frequencies are $f_{11} = 0.289$ THz and $f_{12} = 0.302$ THz.

Besides, ADMs exhibit negative effective index of refraction as Depine and Lakhtakia's Condition (DLC) is satisfied [16], that is, when

$$\varepsilon'_{eff}\,\mu''_{eff} + \varepsilon''_{eff}\,\mu'_{eff} < 0, \qquad (2)$$

where the prime and the double prime denote the real and imaginary part, respectively. The simulation data, reported in Fig. 6, reveals that the first two Mie resonances are excited and lead to negative effective index n_{eff} (shaded area), whose minima is $n_{eff_{min}} = -2.52$ at 0.298 THz, while its bandwidth is 7.1 GHz.

The maximal value of the loss to obtain negative effective index is determined from the DLC. In the case of TiO_2, effective negative index is only achievable as $\tan\delta < 2 \times 10^{-2}$ (see Fig. 7). $\tan\delta < 15 \times 10^{-3}$ has been chosen as the critical value to ensure the negative effective index.

Coupling plays an important role in obtaining a negative index [17]. Indeed, the first two modes of Mie resonance respectively result in a magnetic dipole and an electric one, that interact [18]. Modifying this coupling changes the effective index n_{eff}. For example, modifying one side of the resonators changes the frequencies of the modes of resonances (see equation (1)). Thus, by diminishing the same side of the two resonators of the unit cell, the frequency of the minima of the S_{21}-parameter of the first two modes increase until the two modes are degenerated, having the same frequency [17] (see Fig. 8). Concomitantly, the effective

https://doi.org/10.1017/S1759078725101931 Published online by Cambridge University Press

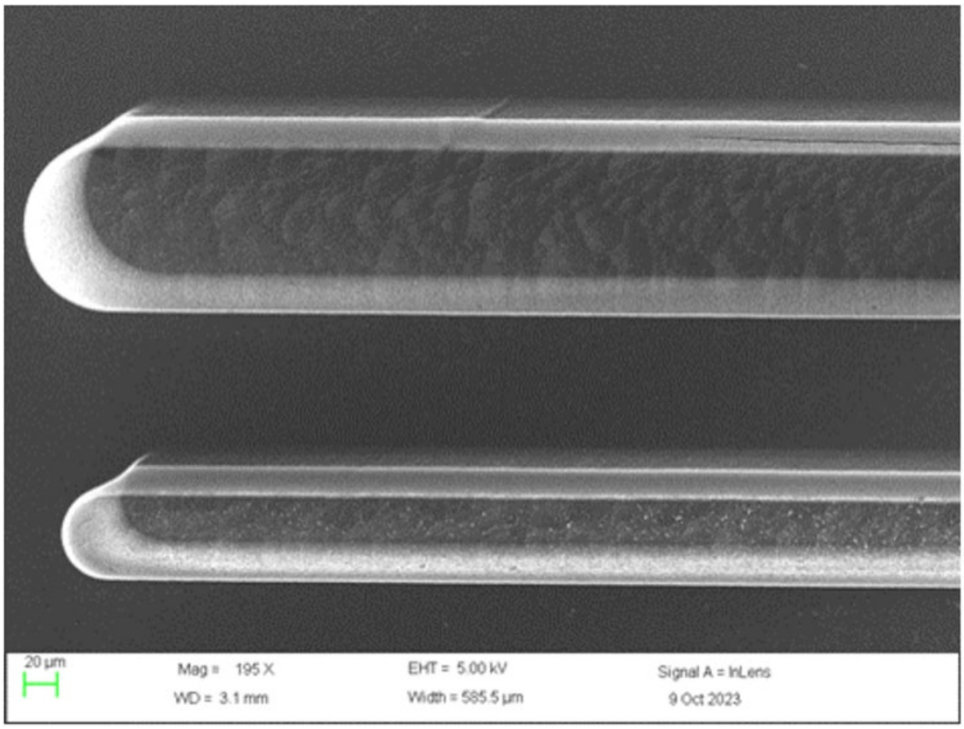


Figure 9. SEM picture of a PMMA mold done by X-ray lithography. Opening dimensions are 110 and 60 μm, respectively, for a depth of 240 μm.

index n_{eff} diminishes as the considered side diminishes, going from near zero values to negative values. As the modes are degenerated, the effective index is no longer defined [19]. A different unit cell, with different sizes but the same EM parameters, leading to a more negative value of the minimum of the $n_{eff_{min}} = -3.6$ at 0.296 THz is reported in [7]. Besides, a similar design and simulation have been carried out at 0.6 THz, also leading to negative effective index (see Fig. 1 in the supplementary material file). In that case, the elementary cell of the ADM comprises two 2D cylinders of TiO_2, one having a rectangular cross-section (28 μm $\times$ 55 μm) and the other having a square cross-section (55 μm $\times$ 55 μm). The cylinders are arranged in a periodic pattern with a period of 120 μm.

Micro-structuration

Our aim is to realize 2D metasurfaces or 3D MM by the micro-structuration of bulk TiO_2. In the fabrication of the devices, particularly for micro-structuring the bulk material, we explored four processes:

(i) micro-molding,
(ii) ICP etching,
(iii) femtosecond laser etching,
(iv) saw cutting.

The three last were carried out on rutile single crystal TiO_2 pellets, with (001) optical axis orientation. Given the dimensions of the resonators, ICP etching is suited for ADMs targeting 0.6 THz, while the others processes are suited for 0.3 THz.

Micro-molding

Micro-molding, using polymer molds, is a microscale manufacturing process. This process has the advantage of facilitating the precise realization of components by accurately reproducing the specific characteristics of a polymer mold.

In this process, the fabrication of a high precision polymethylmethacrylate (PMMA) mold was achieved by the means of deep x-ray lithography (DXRL) technology which can handle the requested high precision, i.e., 1 μm precision for dimension and for positioning between structures (see Fig. 9). The theoretical precision of DXRL is mainly related to the vertical and horizontal divergences of the synchrotron source which are less than 0,1 mrad in our operating conditions, well beyond the required tolerance. X-ray lithography step was performed at Synchrotron SOLEIL, in Saint-Aubin (France) on Metrology beamline which is equipped with at dedicated scanner. The experimental process used is standard [20]. Then the molds are filled with a commercial TiO_2 powder, combined with a binder. The next sintering stage is carried out at high temperature. During this process, the PMMA mold, whose melting point is around 200°C, undergoes combustion, which results in a dense TiO_2 part.

After the sintering, the next step is to extract this metadevice from its base component. This phase involves a meticulous operation to thin the base of the ceramic part, which initially served as the foundation for the patterning. To this end, the patterned side is wrapped in a protective resin matrix, such as epoxy. This epoxy resin layer plays an essential role, not only in keeping the ceramic bars in perfect alignment, but also in protecting them during subsequent operations, such as polishing.

Optical microscope images of a patterned device are reported in Fig. 10. The pattern seen in Fig. 10(a) and (b) is distinguished by a series of ceramic bars. Their width, height and spacing are approximately 130 μm, 80 μm and 75 μm, respectively, which matches the specifications of the PMMA mold used to produce this part. The depth of the LIGA etching was projected to be between 75 and 90 μm. Figure 10(c) displays the 3D measurement of the profile made along the y direction of the pattern. This figure demonstrates

https://doi.org/10.1017/S1759078725101931 Published online by Cambridge University Press

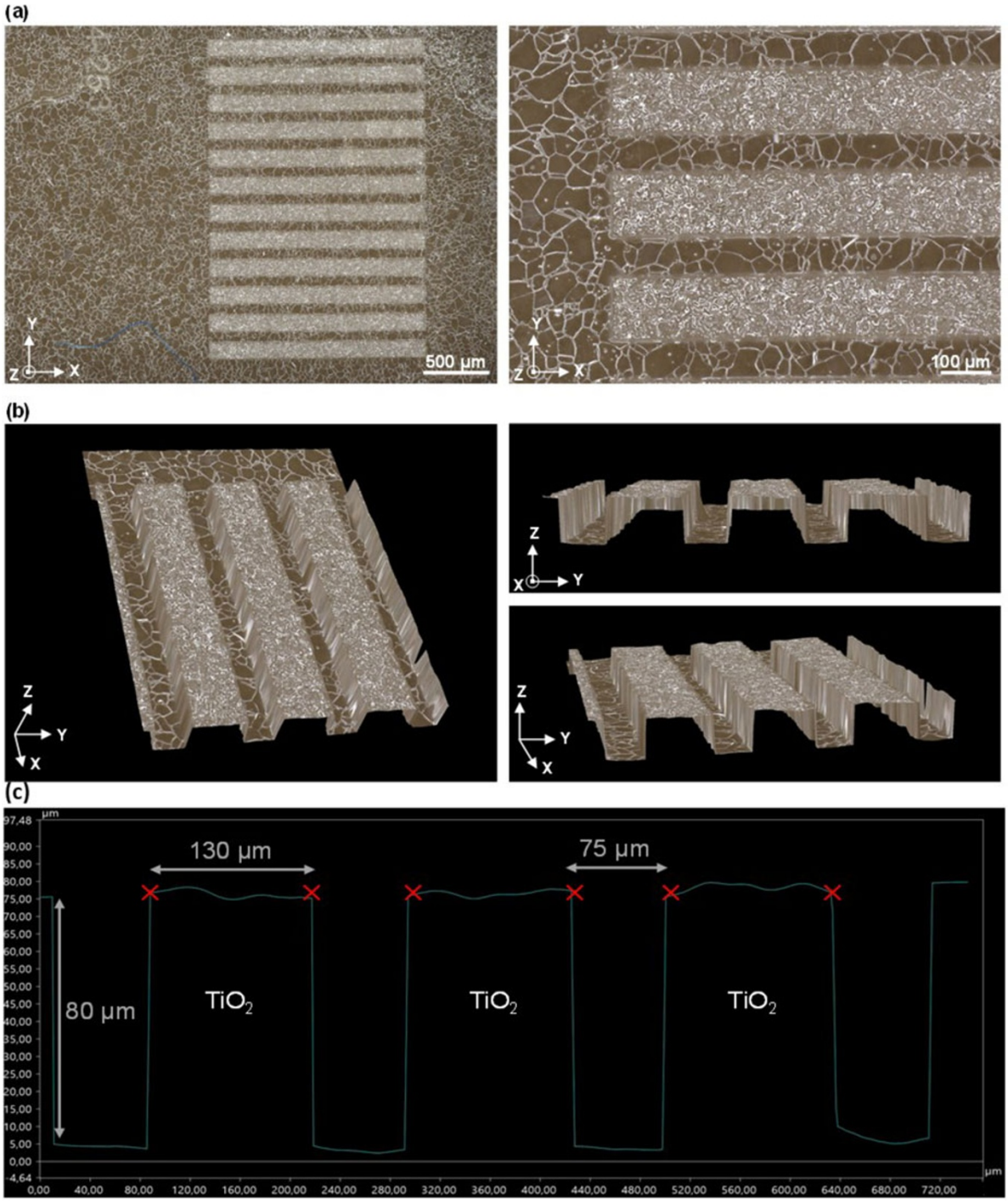


Figure 10. Optical microscope observations (a) in 2D of a TiO_2 pattern structured by micro-molding and (b) 3D reconstruction of a part of the piece. from different viewing angles. (c) 3D measurement profile highlighting the structuration of the bulk material.

that the filling of the micro-cavities was correctly realized during the shaping of the part, with a regular crest height.

Since quartz is transparent in the considered THz range, it can also serve as a mold. The operating principle is the same; however, the mold will not be destroyed during sintering, its melting temperature being sufficiently high. Quartz will consequently serve as a support to the TiO_2 part. We have already fabricated a quartz mold by Inductively Coupled Plasma–Reactive Ion Etching (ICP-RIE) process, similarly to the PMMA one and numerically simulated such an ADM.

Direct etching of TiO_2 by inductively coupled plasma–reactive ion etching (ICP-RIE)

In this process, TiO_2 is etched using a plasma source (ICP-RIE process), in a clean room. This process allows for direct etching of the

https://doi.org/10.1017/S1759078725101931 Published online by Cambridge University Press

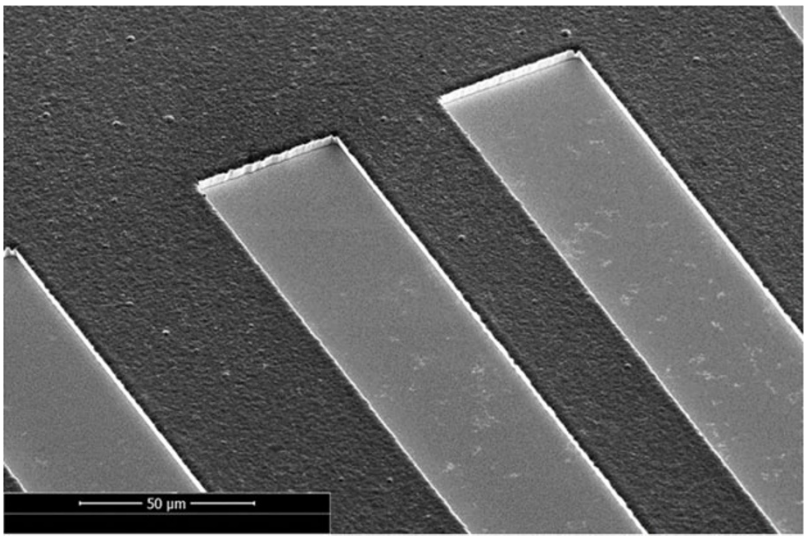
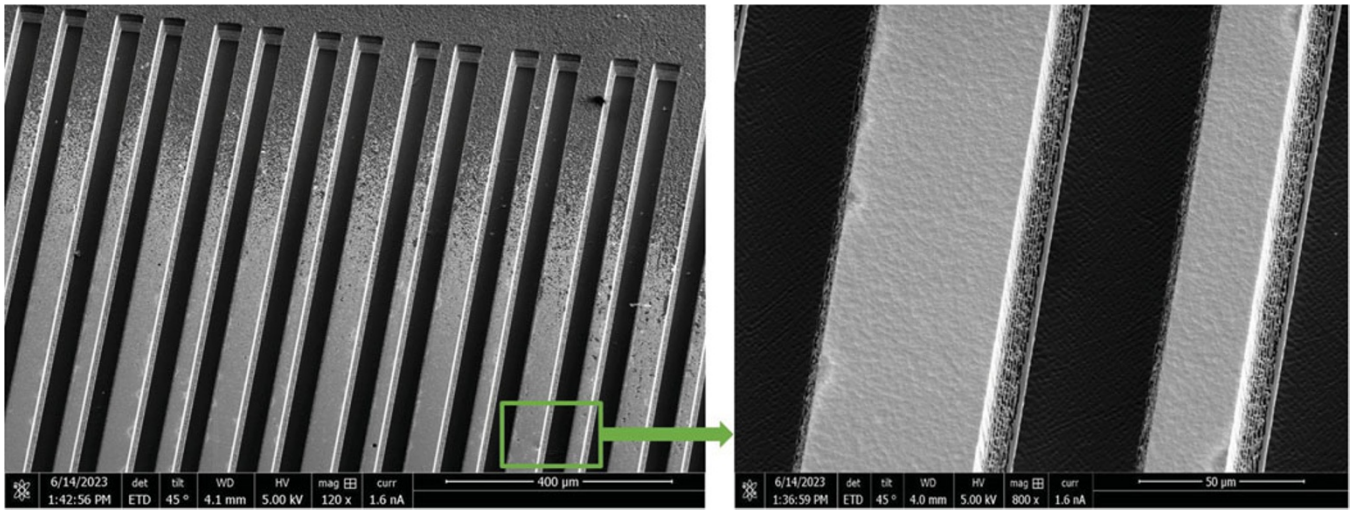
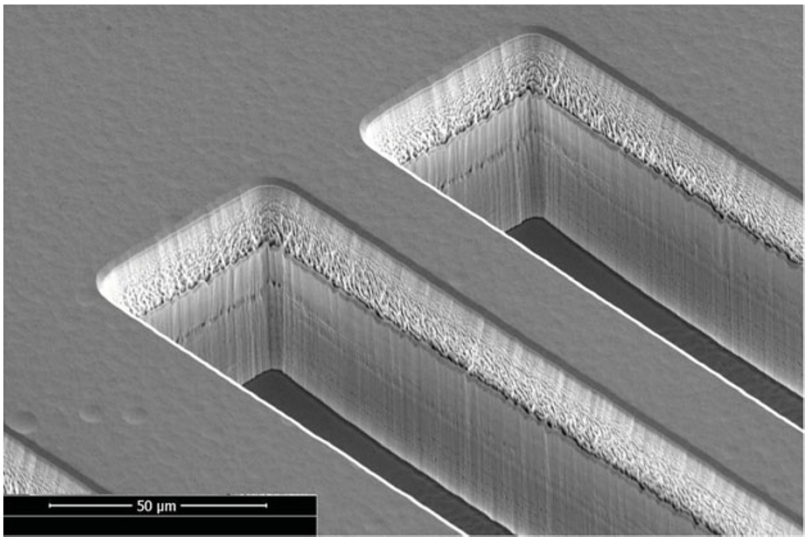


Figure 11. SEM (scanning electron microscopy) image of the patterned Nickel mask deposited on a mono-crystalline TiO_2 pellet to protect it during the ICP-RIE etching.



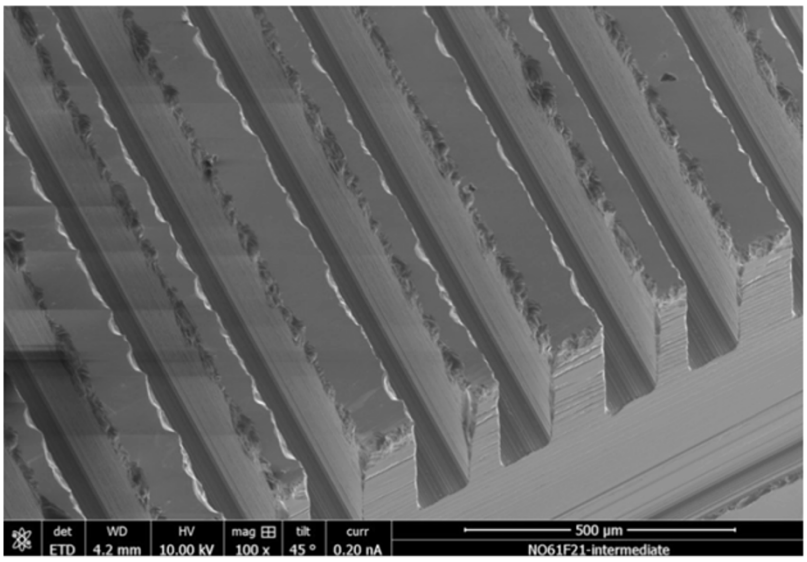
(a) TiO_2 pellet patterned by ICP



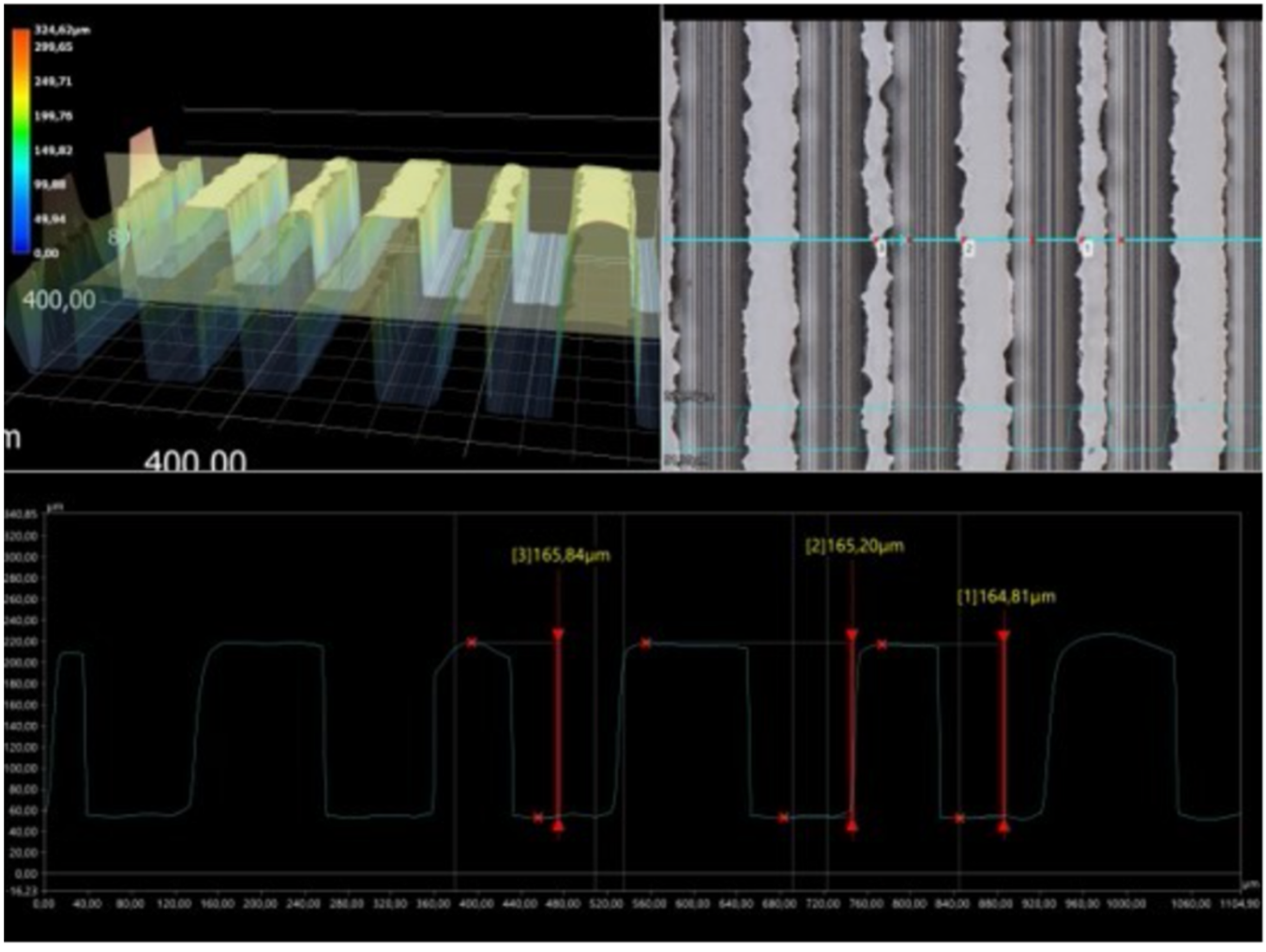
(b) Depth of etching.

Figure 12. SEM (scanning electron microscopy) images of the TiO_2 pellet after 140 min of ICP etching. (a) Left: View of the pattern etched; right: the two bars of the unit cell. (b) Zoom showing the 59 μm high grooves between the TiO_2 bars. From top to bottom: the Ni mask, TiO_2, the passivation layer and the TiO_2 bottom of the grooves. (a) TiO_2 pellet patterned by ICP. (b) Depth of etching.

https://doi.org/10.1017/S1759078725101931 Published online by Cambridge University Press



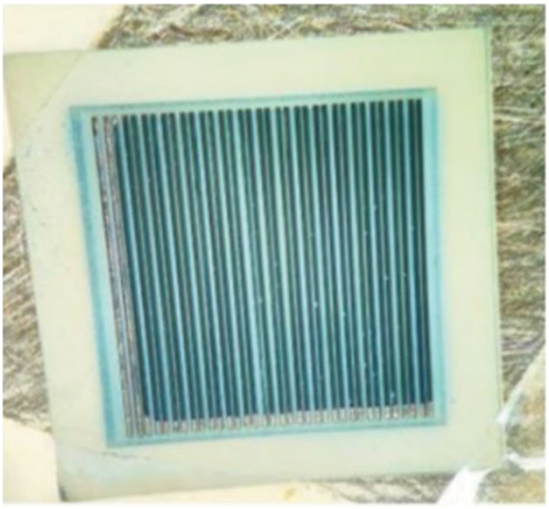
(a) Tilted SEM images of the grooves fabricated on a TiO_2 substrate after removing the protective epoxy layer.



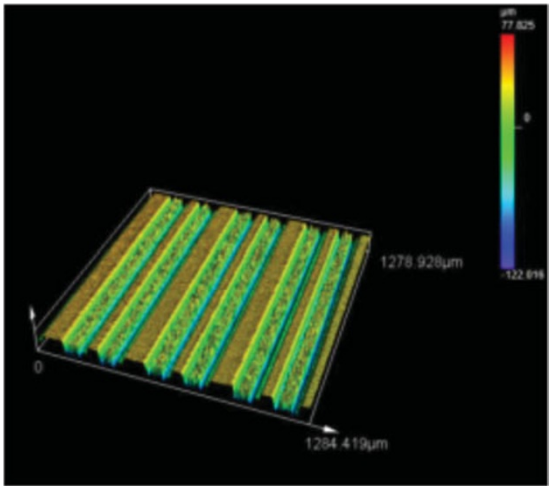
(b) Microscopic 3D Keyence images.

Figure 13. (a) Making grooves in a TiO_2 substrate with a saw. (b) (Top left view): 3D visualization of the pattern cut into the substrate. (Top right view): top view of the sample showing the splinters made in the substrate during the sawing process. (Bottom view): depth profile of the pattern. (a) Tilted SEM images of the grooves fabricated on a TiO_2 substrate after removing the protective epoxy layer. (b) Microscopic 3D Keyence images.

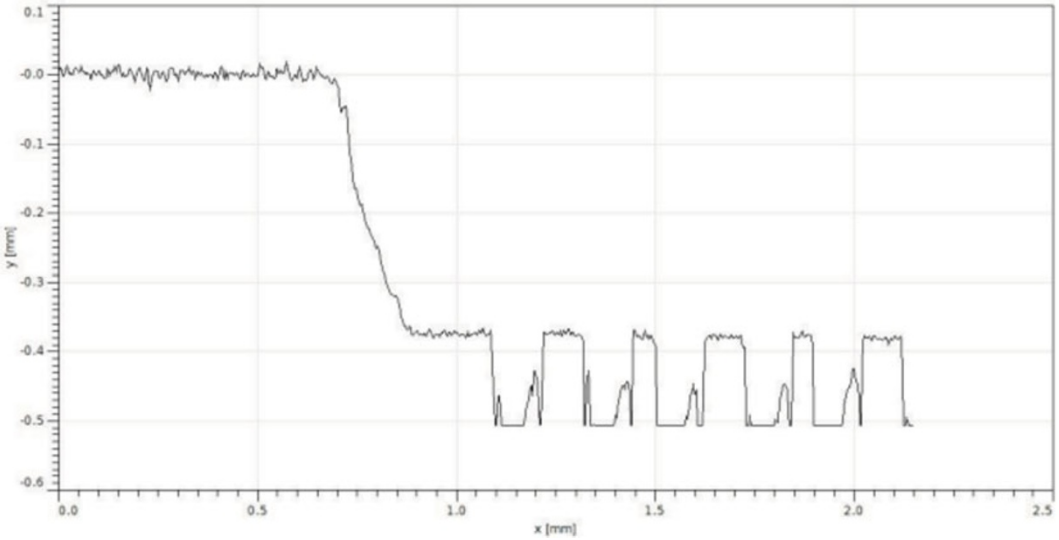
https://doi.org/10.1017/S1759078725101931 Published online by Cambridge University Press



(a) Photography of the mono-crystallin TiO_2 pellet (10×10 cm^2 large and 500 μm thick) engraved and cut by femtosecond laser.



(b) Topography image showing the etched pattern.



(c) Depth profile of the 500 μm thick pellet showing the engraved basin and the cut grooves realizing the pattern of the ADM.

Figure 14. Femtosecond laser etching of a mono-crystalline pellet (Hilase [23]). (a) Photography of the mono-crystallin TiO_2 pellet (10×10 cm^2 large and 500 μm thick) engraved and cut by femtosecond laser. (b) Topography image showing the etched pattern. (c) Depth profile of the 500 μm thick pellet showing the engraved basin and the cut grooves realizing the pattern of the ADM.

https://doi.org/10.1017/S1759078725101931 Published online by Cambridge University Press

desired pattern from the bulk material. Initially, a mono-crystalline TiO_2 pellet (Neyco brand, 500 μm thick and (001) optical axis orientation) is first prepared by depositing a gold layer on the pellet, and then a photosensitive resin. By the means of an optical mask, the resin is exposed to reproduce the desired pattern and then Nickel is electroplated (see Fig. 11), which will protect the intended areas of TiO_2 during exposure to the plasma.

The SEM (scanning electron microscope) images (see Fig. 12) reveal the success of the etching process: indeed an groove depth of 59 μm was etched into the pellet in a 140 min run (see Fig. 12(b)). This result is remarkable since only the etching of a few hundred nanometers in TiO_2 has been reported in the literature [21, 22]. It can be noticed from top to bottom: the Nickel mask, the bulk TiO_2, a passivation layer and the TiO_2 the bottom of the grooves, which have been characterized by Energy-dispersive X-ray spectroscopy (EDX). To finalize the device, polishing its back side of the TiO_2 will be necessary. For a successful operation, the patterned TiO_2 has to be wrapped in epoxy resin, the thickness of which eases handling for subsequent characterizations.

Saw cutting

This micro-structuring was carried out using a DISCO cutting equipment, model DAD 641. This equipment can cut wafers of various types (silicon, GaAs, glass, sapphire, etc.) and of various sizes from 200 to 10 mm^2. The cutting blade is of the diamond resin type. Its thickness is 100 μm and it is cooled under a water jet. One disadvantage of this process is that the grooves between the ceramic bars during cutting is set by the thickness of the blade, which sets the period of the pattern of the unit cell of the ADM. Currently, the thinnest blade available on the market for cutting TiO_2 is 100 μm thick, which roughly corresponds to our needs. To limit splinters, the pellet has been coated with an epoxy resin. The results are shown in Fig. 13 and they demonstrate that this is a reliable and inexpensive process.

Femtosecond laser etching

A TiO_2 pellet has been etched by the means of a laser PERLA 100 (wavelength 1030 nm, power max. 100 W, pulse duration 1.5 ps, repetition rate 100 kHz) at Hilase Center [23]. A square basin with 6.4 mm large sides and 390 μm depth was engraved in a mono-crystallin pellet (10 $\times$ 10 cm^2 large and 500 μm thick). Then, grooves were cut in this basin to realize the 110 μm + 116 μm + 58 μm + 116 μm pattern of TiO_2 bars with a 200 μm period. The height of the bars is 110 μm. A photography of the etched sample and its profile are reported in Fig. 14.

Comparison of the processes

In this section, we compare three of the fabrication processes that can be used to fabricate devices operating at 0.3 THz. Getting the negative index requires the first two Mie resonances, meaning that the TiO_2 bars sustain resonances. Some of their parameters have then to satisfy specific features: tolerance of about 1 μm on bars sides and their verticality has to be the closest to 90°. The opening between two resonators is less important as it plays on the coupling of the modes, which is less strict (see Fig. 8). The tolerance versus the opening at 0.3 THz is reported in Fig. 15, based on estimated values, which shows that the three methods are suitable. Nevertheless, because a cross-section cut is needed, we could only measure the verticality in the case of the saw cutting, which is

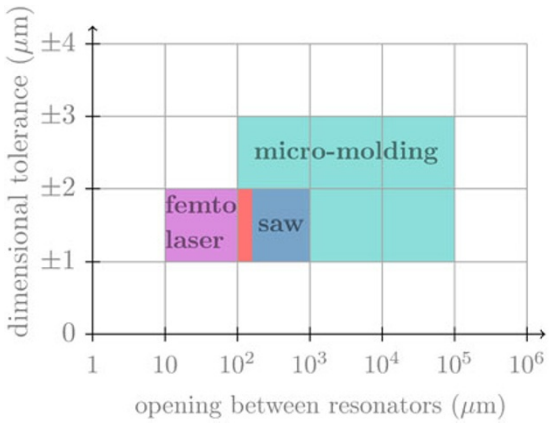


Figure 15. Comparison of the micro-structuring processes at 0.3 THz. The red area is the targeted one.

91°. The verticality is set by that of the mold, as micro-molding is involved.

Besides, because of the achieved etching depth (59 μm) (see section "Femtosecond Laser Etching"), the ICP-RIE process is consequently not currently usable for devices operating at 0.3 THz, whereas it could be at 0.6 THz. Indeed, the characteristic size of the unit cell is about 110 μm at 0.3 THz, and about 55 μm at 0.6 THz.

Conclusion

We have produced TiO_2 ceramic samples for the realization of ADM operating at THz frequencies. By evaluating the two fabrication processes for these ceramics – conventional sintering and SPS – we studied the impact of post-annealing on SPS samples. These samples were characterized using THz TDS in the 0.2 to 1.4 THz spectrum. Our results indicate that the combination of SPS and annealing yields high-density TiO_2 samples with a permittivity of around 100. These possess low losses ($\tan\delta$ less than 2.10^{-2}), making them suitable for ADM.

In addition, we explored four micro-structuring processes:

(i) micro-molding,
(ii) direct TiO_2 etching by ICP,
(iii) saw cutting, and
(iv) femtosecond laser etching.

The obtained results are promising. Micro-molding and saw cutting allows us to achieve vertical and parallel sidewalls. Besides, we have engraved, by ICP-RIE, a TiO_2 pellet up to 59 μm depth, which has not been yet reported. This last process could be suitable for devices operating around 0.6 THz.

Acknowledgements. D.A.D, F.L. and É.A. thank the French RENATECH network (specifically Thomas Tillocher @ GREMI – UMR 7344 CNRS). F.B. would like to thank P. Mercère and P. Da Silva for their support on the Metrology beamline at SOLEIL for the LIGA process.

Funding statement. D.A.D. thanks the MITI (Initiatives Transverses et Interdisciplinaires – CNRS) for financial support. This work has been funded by the French Agence Nationale de la Recherche (ANR) under DisPonT project.

Competing interests. None declared.

References

1. **Luo W, Yan S and Zhou J** (2022) Ceramic-based dielectric metamaterials. *Interdisciplinary Materials* **1**(1), 11–27.
2. **Dupas C, Guillemet-Fritsch S, Geffroy PM, Chartier T, Baillergeau M, Mangeney J, Roux JF, Ganne JP, Marcellin S, Degiron A and Akmansoy É** (2018) High permittivity processed $SrTio_3$ for metamaterials applications at terahertz frequencies. *Scientific Reports* **8**(1), 15275.
3. **Matsumoto N, Nakagawa T, Kageyama K, Wada N and Sakabe Y** (2006) Terahertz band-pass filter fabricated by multilayer ceramic technology. *Japanese Journal of Applied Physics* **45**(9S), 7499.
4. **Saponjic ZV, Dimitrijevic NM, Tiede DM, Goshe AJ, Zuo X, Chen LX, Barnard AS, Zapol P, Curtiss L and Rajh T** (2005) Shaping nanometer-scale architecture through surface chemistry. *Advanced Materials* **17**(8), 965–971.
5. **Lemaire PC and Parsons GN** (2017) Thermal selective vapor etching of TiO2: Chemical vapor etching via WF6 and self-limiting atomic layer etching using WF6 and BCl3. *Chemistry of Materials* **29**(16), 6653–6665.
6. **Choi KR, Woo JC, Joo YH, Chun YS and Kim CI** (2013) Dry etching properties of TiO_2 thin films in o2/cf4/ar plasma. *Vacuum* **92**, 85–89.
7. **Djemmah DA, Gourdonnaud D, Geffroy P-M, Roux J-F, Bouamrane F and Akmansoy E** (2024) From bulk toward micro-structured TiO_2 ceramics for all-dielectric metamaterials at terahertz frequencies In *2024 18th European Conference on Antennas and Propagation (EuCAP)*, pp. 1–5. https://doi.org/10.23919/EuCAP60739.2024.10501288.
8. https://teraview.com/terapulselx/.
9. **Roux JF, Garet F and Coutaz JL** (2014) Principles and applications of THz time domain spectroscopy. In *Physics and applications of terahertz radiation*. Dordrecht: Springer Netherlands, pp. 203–231.
10. **Duvillaret L, Garet F and Coutaz JL** (1996) A reliable method for extraction of material parameters in terahertz time-domain spectroscopy. *IEEE Journal of Selected Topics in Quantum Electronics* **2**(3), 739–746.
11. **Yu C, Zeng Y, Yang B, Donnan R, Huang J, Xiong Z, Mahajan A, Shi B, Ye H, Binions R and Tarakina NV** (2017) Titanium dioxide engineered for near-dispersionless high terahertz permittivity and ultra-low-loss. *Scientific Reports* **7**(1), 6639.
12. **Matsumoto N, Hosokura T, Kageyama K, Takagi H, Sakabe Y and Hangyo M** (2008) Analysis of dielectric response of TiO_2 in terahertz frequency region by general harmonic oscillator model. *Japanese Journal of Applied Physics* **47**(9S), 7725.
13. **Djemmah DA, Geffroy P-M, Chartier T, Roux J-F, Bouamrane F and Akmansoy E** (2022) Processing high permittivity TiO_2 for all-dielectric metamaterials applications at terahertz frequencies. In *Proceedings of the Sixth International Symposium on Dielectric Materials and Applications (ISyDMA6)*. Cham: Springer International Publishing, pp. 177–183.
14. **Setvín M, Wagner M, Schmid M, Parkinson GS and Diebold U** (2017) Surface point defects on bulk oxides: Atomically-resolved scanning probe microscopy. *Chemical Society Reviews* **46**(7), 1772–1784.
15. **Cohn SB** (2003) Microwave bandpass filters containing High-Q dielectric resonators. *IEEE Transactions on Microwave Theory and Techniques* **16**(4), 218–227. https://doi.org/10.1109/TMTT.1968.1126654.
16. **Depine RA and Lakhtakia A** (2004) A new condition to identify isotropic dielectric-magnetic materials displaying negative phase velocity. *Microwave and Optical Technology Letters* **41**(4), 315–316.
17. **Akmansoy E and Marcellin S** (2018) Negative index and mode coupling in all-dielectric metamaterials at terahertz frequencies, *EPJ Applied Metamaterials* **5**(10), 9. https://doi.org/10.1051/epjam/2018006.
18. **Lepetit T, Akmansoy E and Ganne J-P** (2011) Experimental evidence of resonant effective permittivity in a dielectric metamaterial. *Journal of Applied Physics* **109**(2), 023115.
19. **Szabó Z, Park G-H, Hedge R and Li E-P** (2010) A unique extraction of metamaterial parameters based on Kramers-Kronig relationship. *IEEE Transactions on Microwave Theory and Techniques* **58**(10), 2646–2653. https://doi.org/10.1109/TMTT.2010.2065310.
20. **Bellanger C, Brignon A, Toulon B, Primot J, Bouamrane F, Bouvet T, Megtert S, Quetel L and Allain T** (2011) Design of a fiber-collimated array for beam combining. *Optical Engineering* **50**(2), 025005. https://doi.org/10.1117/1.3537968.
21. **Joo Y-H, Woo J-C and Kim CI** (2012) Dry etching properties of TiO_2 thin film using inductively coupled plasma for resistive random access memory application. *Transactions on Electrical and Electronic Materials* **13**(3), 144–148. https://doi.org/10.4313/TEEM.2012.13.3.144.
22. **Park M, Yoon I and Yeonsang EP** (2022) Etching for vertical sidewall formation in TiO_2 nanorods. *Applied Science and Convergence Technology* **31**(5), 113–115.
23. **HiLASE Centre Institute of Physics of the Czech Academy of Sciences** https://www.hilase.cz/en/.



Djihad Amina Djemmah received a Master's degree in Nanoscience and a PhD from Paris-Saclay University in 2020 and 2024, respectively. She is currently a postdoctoral researcher at the Institut des Nanotechnologies de Lyon (INL), where her work focuses on the development and optimization of advanced fabrication processes for nanoscale devices.



Fayçal Bouamrane, CNRS research engineer at Laboratoire Albert Fert, graduated in 1991 from the national engineering school, ENSI in Caen, France, in the field of materials science. He received a PhD degree from University Paris XI Orsay, in 1997, in materials science. Since 1998 he is using and developing the Deep X-Ray Lithography (DXRL) and related LIGA activity (German acronym for lithography, electrogrowth and molding). He is responsible of the lithography LIGA beam line at synchrotron SOLEIL since 2009. His research activity is focused on fabrication of X-rays dedicated micro-structures, in the field of THz technology as optical devices (multiplexers…) and more recently in processing all-dielectric meta-materials.



J.-F. Roux obtained his PhD from Grenoble University in 1995. In 1996, he became Associate Professor at the Université Savoie Mont Blanc (USMB) in the Department of Electrical Engineering. After defending his Habilitation in 2010, he was promoted to Professor in 2021. As a member of the CROMA laboratory (USMB, G-INP, UGA, CNRS), his research focuses both on optoelectronic components for THz signal generation and detection, and on the characterization of materials and devices for applications at THz frequencies. He is currently in charge of the Photonics Optics and Terahertz Optoelectronics group within this laboratory.



P.-M. Geffroy received his Ph.D. at the University of Bordeaux in 2005. He became researcher at French National Centre of Scientific Research (CNRS) at Institut of Research on Ceramics (IRCER) in 2006, and he is responsible of ceramic process research group at IRCER since 2020, as senior researcher. He is active in the study of innovative shaping processes and ceramic materials.



E. Akmansoy obtained his PhD and his Habilitation à Diriger des Recherche (HDR) from Université Paris-Saclay (Université Paris-Sud), where he is Associate Professor. He develops his research themes, which are about Photonic Crystals devices and Metamaterials, at the Centre de Nanosciences and Nanotechnologies (UMR 9001-CNRS).

https://doi.org/10.1017/S1759078725101931 Published online by Cambridge University Press